Contents lists available at ScienceDirect

Ore Geology Reviews

journal homepage: www.elsevier.com

Origin and evolution of mineralizing fluids and exploration of the Cerro Quema Au-Cu deposit (Azuero Peninsula, Panama) from a fluid inclusion and stable isotope perspective

Isaac Corral [a, b, *], Esteve Cardellach [a], Mercè Corbella [a], Àngels Canals [c], Albert Griera [a], David Gómez-Gras [a], Craig A. Johnson [d]

[a] *Departament de Geologia, Universitat Autònoma de Barcelona, 08193, Barcelona, Spain*
[b] *EGRU (Economic Geology Research Centre), College of Science, Technology and Engineering, James Cook University, Townsville, QLD 4811, Australia*
[c] *Facultat de Geologia, Universitat de Barcelona. 08028, Barcelona, Spain*
[d] *U.S. Geological Survey, Denver, CO 80225. USA*

ARTICLE INFO

Article history:
Received 3 April 2016
Accepted 5 September 2016
Available online xxx

Keywords:
Cerro Quema
fluid inclusions
stable isotopes
alunite-pyrite
exploration

ABSTRACT

Cerro Quema is a high sulfidation epithermal Au-Cu deposit with a measured, indicated and inferred resource of 35.98 Mt. @ 0.77 g/t Au containing 893,600 oz. Au (including 183,930 oz. Au equiv. of Cu ore). It is characterized by a large hydrothermal alteration zone which is interpreted to represent the lithocap of a porphyry system. The innermost zone of the lithocap is constituted by vuggy quartz with advanced argillic alteration locally developed on its margin, enclosed by a well-developed zone of argillic alteration, grading to an external halo of propylitic alteration. The mineralization occurs in the form of disseminations and microveinlets of pyrite, chalcopyrite, enargite, tennantite, and trace sphalerite, crosscut by quartz, barite, pyrite, chalcopyrite, sphalerite and galena veins.

Microthermometric analyses of two phase (L + V) secondary fluid inclusions in igneous quartz phenocrysts in vuggy quartz and advanced argillically altered samples indicate low temperature (140–216 °C) and low salinity (0.5–4.8 wt% NaCl eq.) fluids, with hotter and more saline fluids identified in the east half of the deposit (Cerro Quema area).

Stable isotope analyses (S, O, H) were performed on mineralization and alteration minerals, including pyrite, chalcopyrite, enargite, alunite, barite, kaolinite, dickite and vuggy quartz. The range of $\delta^{34}S$ of sulfides is from − 4.8 to − 12.7‰, whereas $\delta^{34}S$ of sulfates range from 14.1 to 17.4‰. The estimated $\delta^{34}S_{\Sigma S}$ of the hydrothermal fluid is − 0.5‰. Within the advanced argillic altered zone the $\delta^{34}S$ values of sulfides and sulfates are interpreted to reflect isotopic equilibrium at temperatures of ~ 240 °C. The $\delta^{18}O$ values of vuggy quartz range from 9.0 to 17.5‰, and the $\delta^{18}O$ values estimated for the vuggy quartz-forming fluid range from − 2.3 to 3.0‰, indicating that it precipitated from mixing of magmatic fluids with surficial fluids. The $\delta^{18}O$ of kaolinite ranges from 12.7 to 18.1‰ and δD from − 103.3 to − 35.2‰, whereas the $\delta^{18}O$ of dickite varies between 12.7 and 16.3‰ and δD from − 44 to − 30. Based on $\delta^{18}O$ and δD, two types of kaolinite/dickite can be distinguished, a supergene type and a hypogene type. Combined, the analytical data indicate that the Cerro Quema deposit formed from magmatic-hydrothermal fluids derived from a porphyry copper-like intrusion located at depth likely towards the east of the deposit. The combination of stable isotope geochemistry and fluid inclusion analysis may provide useful exploration vectors for porphyry copper targets in the high sulfidation/lithocap environment.

© 2016 Published by Elsevier Ltd.

1. Introduction

The Azuero Peninsula in southwestern Panama shows evidence of widespread hydrothermal activity as indicated by the existence of several Au-Cu mineral occurrences including the Cerro Quema high sulfidation epithermal Au-Cu deposit (Fig. 1). The Cerro Quema deposit was discovered in 1988 by the Compañía de Exploración Minera S. A. (CEMSA) during geological and metallogenetic studies by the United Nations Development Program (UNDP; 1965), and today is one of the most prospective exploration projects in Panama. The Cerro Quema deposit consists of several mineralized zones: from east to west, Cerro Quema, Cerro Quemita, and La Pava (Fig. 2). The measured, indicated and inferred resources as of 2014 are 35.98 Mt. @ 0.77 g/t Au containing a total of 893,600 troy ounces Au of which 183,930 troy ounces are gold equivalent of the contained copper (Sutcliffe et al., 2014). Additional mineralized bodies are found to the east —the Cerro Idaida, East Quema Jungle, and Cerro Pelona prospects— but the Au and Cu grade and content of these prospects have not yet been determined.

The first geological studies of the Azuero Peninsula (e.g., Del Giudice and Recchi, 1969; Ferencic, 1970; Kesler et al., 1977) noted the potential for Au and Cu deposits in the region. Later works specifically on the Cerro Quema deposit focused on geology (Horlacher and Lehmann, 1993; Nelson, 1995; Corral et al., 2011), and metallogeny (Leach, 1992; Corral, 2013; Corral et al., *2016*). This report presents the first documentation of the genesis of the de-

* *Corresponding author.
Email address: I.Corral.Geo@gmail.com (I. Corral)

http://dx.doi.org/10.1016/j.oregeorev.2016.09.008
0169-1368/© 2016 Published by Elsevier Ltd.

UNCORRECTED PROOF

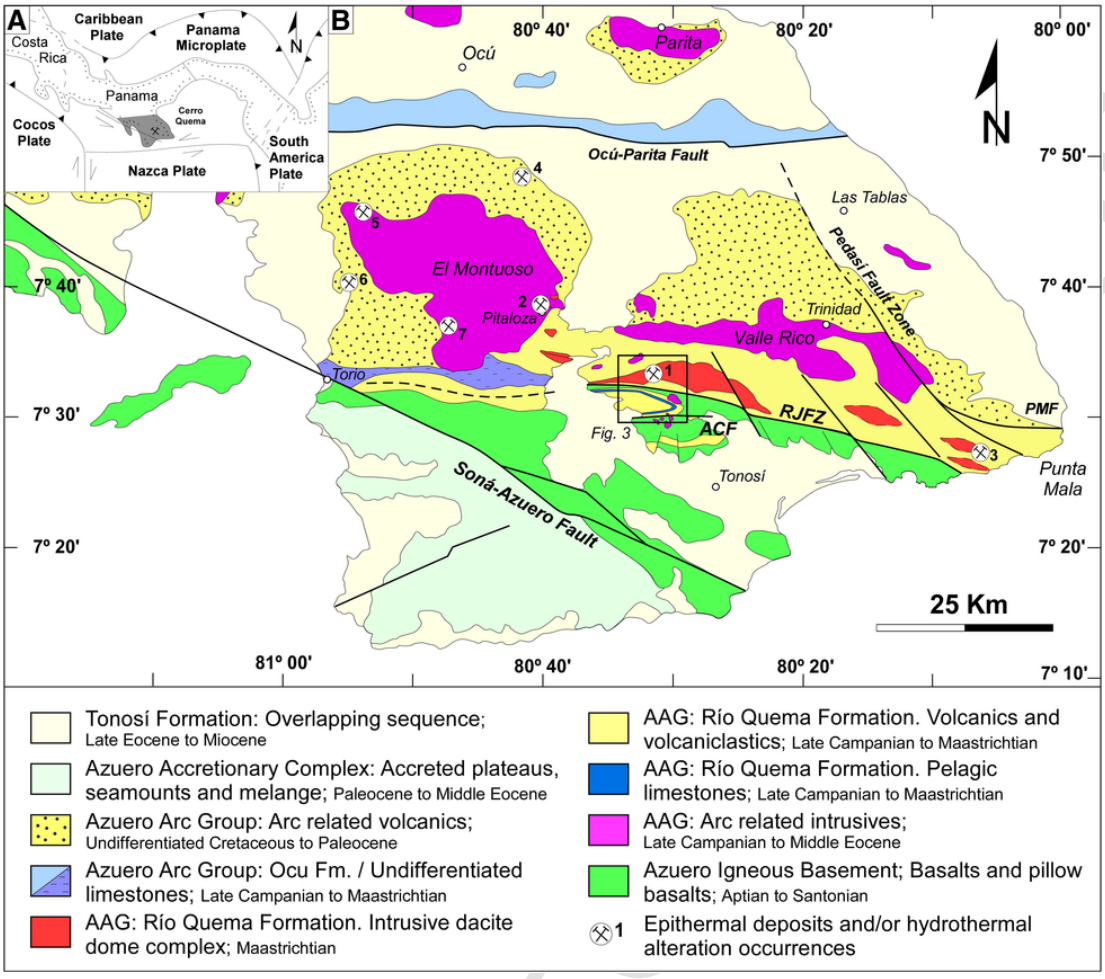

Fig. 1. A) Plate tectonic setting of south Central America. B) Simplified geological map of the Azuero Peninsula and mineral occurrences. AAG: Azuero Arc Group, ACF: Agua Clara Fault, PMF: Punta Mala Fault, RJFZ: Río Joaquín Fault Zone (After Dirección General de Rercursos Minerales (DGRM) (1976); Buchs et al., 2010; Corral et al., 2011, 2013). Mineral ocurrences: 1) Cerro Quema, 2) Pitaloza, 3) Juan Díaz, 4) Las Minas, 5) Quebrada Barro, 6) Quebrada Iguana, 7) Cerro Viejo.

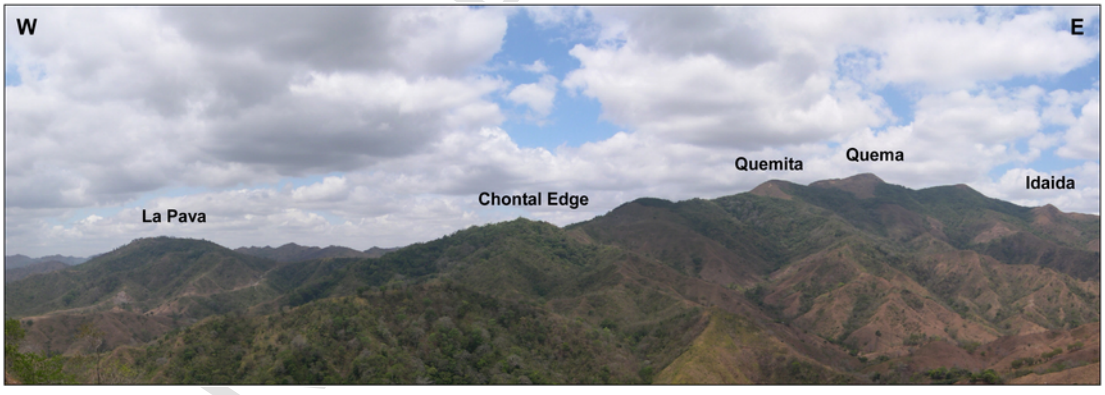

Fig. 2. Overview of Cerro Quema including La Pava, Cerro Quemaita, Cerro Quema and Cerro Idaida ore zones.

posit as indicated by the study of the origin and evolution of the ore fluids.

Here we present the results of fluid inclusion and stable isotope studies undertaken to determine the origin of the fluids responsible for ore deposition. The results are integrated into a genetic model of high sulfidation Au-Cu deposits (c.f., Arribas, 1995). The results also

provide exploration vectors for underlying porphyry copper targets, vectors that may be useful elsewhere in terranes with similar geology.

2. Regional Geology

Panama is underlain by the youngest segment of the land bridge that joins the North and South American plates. The geology consists of a volcanic arc that developed in Late Cretaceous to Paleocene time during subduction of the ancient Farallon plate beneath the Caribbean plate. The resulting tectonic block lies at the junction of the Caribbean, South American, Cocos, and Nazca plates (e.g., Duque-Caro, 1990; Kellogg et al., 1995; Harmon, 2005; Fig. 1). The Azuero Peninsula in southwestern Panama represents the Panamanian portion of the arc. Major tectonic structures include the northwest trending Soná-Azuero Fault zone and the east trending Ocú-Parita, Agua Clara, and Río Joaquín Fault Zones (Kolarsky et al., 1995; Buchs, 2008; Corral et al., 2011, 2013; Fig. 1).

In the Azuero Peninsula the different geodynamic stages are reflected in seven main lithostratigraphic units: 1) the Azuero Igneous Basement, a series of pillow and flow basalts of Coniacian – Early Santonian age (~ 89–85 Ma; Kolarsky et al., 1995; Lissinna, 2005; Buchs et al., 2009, 2010); 2) the Río Quema Formation, a volcano-sedimentary sequence of Campanian to Maastrichtian age (~ 71 to 66 Ma; Wegner et al., 2011; Corral et al., 2013, 2016) that represents the initial stage of the arc; 3) the Cretaceous El Montuoso I-type batholith (~ 69 to 65 Ma; Del Giudice and Recchi, 1969; Kesler et al., 1977; Montes et al., 2012; Corral et al., 2016), which corresponds to arc-related plutonism; 4) the Lower Eocene volcanic arc, which developed on top of the Cretaceous arc and corresponds to the Valle Rico I-type batholith (~ 55 to 49 Ma; Del Giudice and Recchi, 1969; Lissinna, 2005; Montes et al., 2012; Corral et al., 2016); 5) the Parita batholith, Middle Eocene volcanic arc located north of the Cretaceous-Lower Eocene volcanic arc (~ 45 Ma; Lissinna, 2005; Montes et al., 2012; Corral et al., 2016) (Fig. 1); 6) the Paleocene to Middle Eocene seamounts, oceanic plateaus and a mélange accreted along the ancient subduction trench, which represents the accretionary complex (Hoernle et al., 2002; Lissinna, 2005; Hoernle and Hauff, 2007; Buchs et al., 2011); and 7) the Tonosí Formation, the youngest overlapping sedimentary sequence of Middle Eocene - Early Miocene age (Recchi and Miranda, 1977; Kolarsky et al., 1995; Krawinkel et al., 1999).

3. Geology of the deposit

3.1. Geology

The Cerro Quema high sulfidation epithermal Au-Cu deposit is located in the center of the Azuero Peninsula, and covers an area of ~ 20 km^2 (Figs. 1, 3). The mineralization is hosted in the dacite dome complex of the Río Quema Formation, a late Campanian to Maastrichtian volcanic sequence that outcrops in the central and southeastern parts of the Peninsula. The Rio Quema Formation is bounded to the north by a series of diorite and quartz diorite batholiths (e.g., the El Montuoso and Valle Rico batholiths) and to the south by the Azuero Igneous Basement. The Cerro Quema deposit is estimated to be early Eocene in age and may be related to subvolcanic porphyry intrusions contemporaneous with the Valle Rico batholith (~ 55–49 Ma; Corral et al., 2016).

In the study area, the Río Quema Formation overlies the Azuero Igneous Basement and is discordantly overlapped by the Tonosí Formation. The unit is affected by an extensive network of faults, predominantly normal faults with northwest- and northeast-trend, subvertical dips, and occasional strike slip components. In addition, mesoscale southwest-plunging open folds with moderately dipping limbs are observed in the area (Fig. 3). Deformation indicators (e.g., tension gashes, cataclasites, etc.) are observed mostly in the northern area, whereas a kilometer-scale east-trending syncline characterizes the southern area (Fig. 3). Overall, the structures suggest dextral transpression with dominant reverse dip-slip motion during late Campanian to middle Eocene time (Corral et al., 2013).

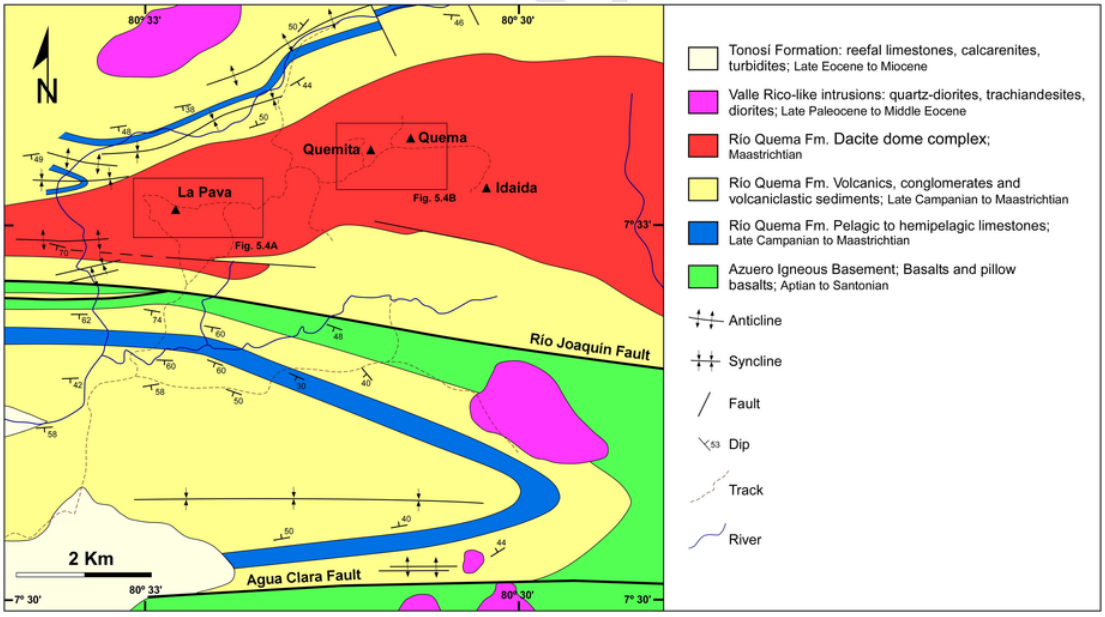

Fig. 3. Simplified geologic map map of Central Azuero Peninsula, and location of the Cerro Quema deposit (modified from Corral et al., 2011, 2013).

EDITED PROOF

3.2. Hydrothermal alteration

The hydrothermal alteration at Cerro Quema follows an eastward trend that is parallel to secondary faults of the Río Joaquín Fault Zone. It defines concentric alteration halos which, in cross-section, are mushroom-shaped (e.g., La Pava; Fig. 4). Water vapor permeability and porosity of different volcanic rocks of the Río Quema Formation have been measured, obtaining values for dacite rocks (permeability of $2.0 \cdot 10^{-11}$ kg/s*m·Pa and 10.8% of porosity), andesite rocks (permeability of $5.1 \cdot 10^{-12}$ kg/s*m·Pa and 7.4% of porosity) and basalt rocks (permeability of $1.7 \cdot 10^{-11}$ kg/s*m·Pa and 6.4% of porosity). Wall-rock alteration at Cerro Quema is mainly restricted to the dacite domes of the Río Quema Formation, which have higher porosity and permeability than other rock types of the volcano-sedimentary sequence.

Four distinct alteration zones have been identified at Cerro Quema on the basis of field mapping, logging, and on analysis of surface and drill core samples by optical microscopy, X-ray diffraction analysis, and scanning electron microscopy-energy dispersive spectroscopy (Fig. 4). Several vuggy quartz centers (up to ~ 600 m in length) and local advanced argillic alteration zone (up to ~ 250 m in length), are enclosed by an argillic alteration zone (up to ~ 1900 m in length). Propylitic alteration has been observed only in a few drill-core samples, and forms a halo surrounding argillic alteration zone.

Vuggy quartz consists of a groundmass of microcrystalline anhedral grains with disseminated pyrite, chalcopyrite, enargite, tennantite, barite, minor rutile, and trace sphalerite. The advanced argillic alteration zone is characterized by quartz, alunite, natroalunite, aluminium-phosphate-sulfate minerals (APS), dickite, pyrophyllite,

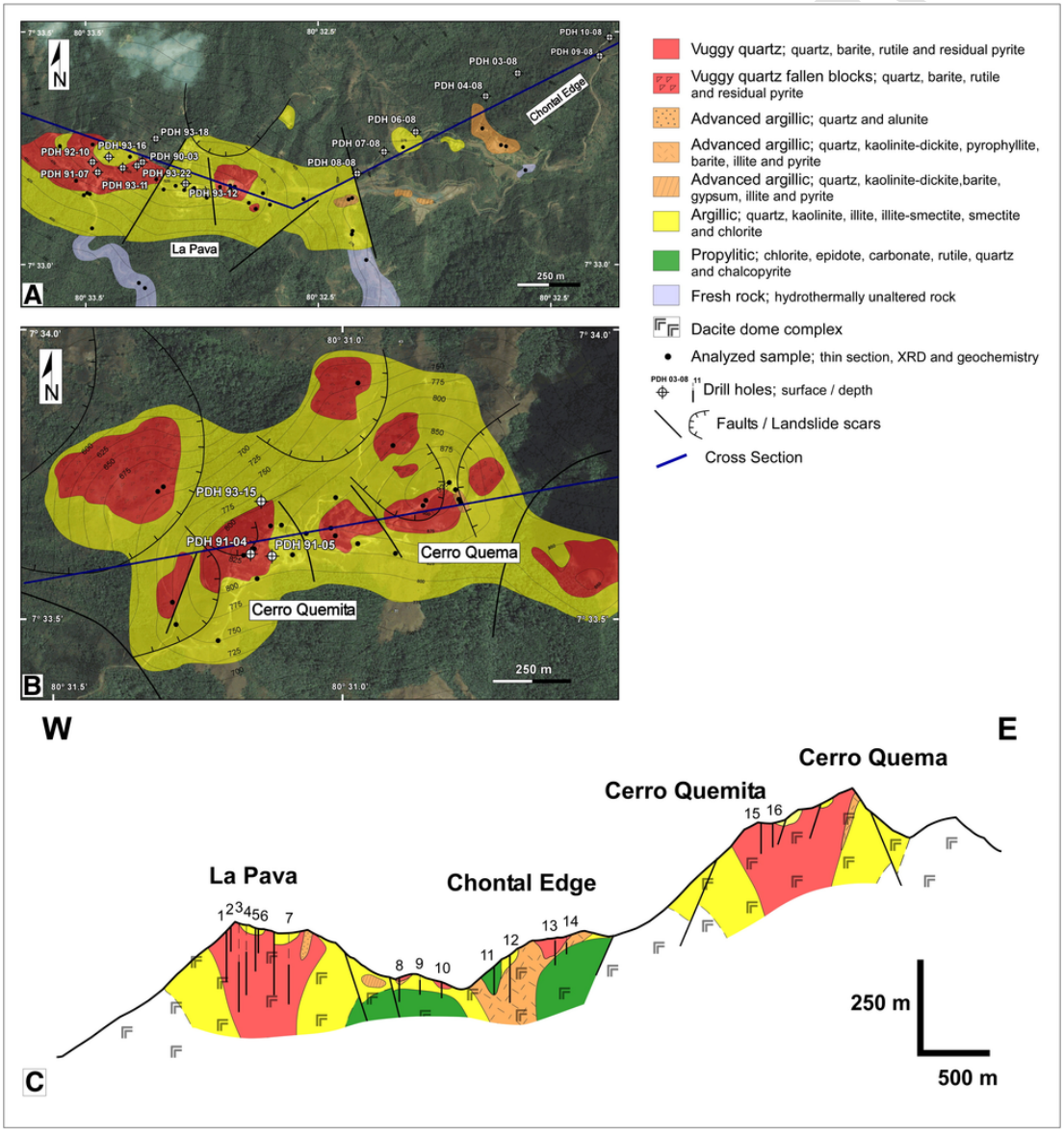

Fig. 4. Cerro Quema hydrothermal alteration maps and cross section; A) La Pava orebody and Chontal Edge zone. B) Cerro Quemita and Cerro Quema orebodies. C) Interpretation of hydrothermal alteration at depth based on drill holes; 1: PDH 92–10, 2: PDH 91–07, 3: PDH 93–16, 4: PDH 93–11, 5: PDH 93–22, 6: PDH 90–03, 7: PDH 93–12, 8: PDH 08–08, 9: PDH 07–08, 10: PDH 06–08, 11: PDH 04–08, 12: PDH 03–08, 13: PDH 09–08, 14: PDH 10–08, 15: PDH 91–04, 16: PDH 93–15.

barite, illite, and minor diaspore and rutile. Argillic alteration produced quartz, kaolinite, illite, illite-smectite, and minor chlorite with local disseminated pyrite. The propylitic alteration zone is characterized by chlorite, epidote, carbonate, rutile, pyrite, chalcopyrite, and minor hematite and magnetite.

Intense weathering, typical of tropical latitudes, has affected fresh and hydrothermally altered rocks in the Cerro Quema area to depths up to 150 m. Weathering of the deposit produced a thick quartz- and iron oxide-rich zone (well-developed on the vuggy quartz alteration) that overprints the primary sulfide-bearing zone.

3.3. Mineralization

The gold and copper mineralization is mainly associated with sulfides occurring in the vuggy quartz and advanced argillic alteration zones. Sulfides (± Au-Cu) formed during hydrothermal alteration, as indicated by: 1) the occurrence of disseminated sulfides in the groundmass of hydrothermally altered rocks, 2) the coprecipitation of sulfides and alteration minerals (e.g., alunite, dickite) in the cement of hydraulic breccias, and 3) the occurrence of sulfides filling fissures and in stockworks and voids of hydrothermally altered rocks (e.g., within the vuggy quartz).

Gold occurs as disseminated submicroscopic grains and as invisible gold within pyrite. Copper is found in chalcopyrite, enargite, bornite, tennantite, covellite and chalcocite, the latter two interpreted to be of supergene origin.

Mineralization can be divided into six stages (Corral et al., 2016; Fig. 5), where stages 3 and 4 are the main ore-forming stages. Stage 1 consists of disseminated pyrite along with rutile and barite in voids and groundmass with minor chalcopyrite, enargite, tennantite, and trace sphalerite (Fig. 6A). Stage 2 is defined by a disseminated pyrite and chalcopyrite in the cement of hydraulic breccia associated with alunite-natroalunite and dickite (Fig. 6B). Stage 3 consists of pyrite, chalcopyrite, enargite and tennantite veinlets that crosscut Stages 1 and 2 (Fig. 6C). Replacement of pyrite by enargite, enargite by tennantite, and tennantite by chalcopyrite can be observed in the veinlets. Stage 4 is found in breccia bands (~ 5 cm thick) composed of pyrite and minor chalcopyrite and enargite. These bands crosscut all previous stages (Fig. 6D). Stage 5 reflects intermediate sulfidation mineralization as compared to high sulfidation in the previous stages. They are characterized by up to 10 cm wide veins containing pyrite, quartz and barite with minor chalcopyrite, sphalerite and galena. Stage 6 is represented by supergene mineralization which developed an oxide zone and an enrichment zone. The oxide zone is characterized by hematite and goethite, replacing the cement of hydrothermal breccias and filling voids in the vuggy quartz zone. Residual hypogene pyrite, barite and rutile are trace minerals in the oxide zone. At the base of the oxide zone secondary Cu-bearing minerals such as chalcocite and minor covellite constitute a zone of supergene enrichment. Secondary Cu-sulfides replace chalcopyrite, tennantite and enargite and also fill submillimeter-scale fractures.

4. Fluid inclusion study

4.1. Sampling and analytical methods

Fluid inclusion studies were carried out on six samples of the vuggy quartz and advanced argillic alteration zones of the Cerro Quema deposit, from surface and drill core samples. All microthermometric analyses were performed on fluid inclusions trapped in igneous quartz phenocrysts from the dacites of the Río Quema Formation (Fig. 7A). Due to small sizing, no fluid inclusions were found in the microcrystalline quartz formed during hydrothermal alteration (e.g., vuggy quartz alteration). Microthermometry was performed at the Universitat Autònoma de Barcelona fluid inclusion laboratory. Measurements were made on doubly polished thin sections (about 100 μm thick) using a Linkam THMSG-600 heating-freezing stage. The equipment was previously calibrated from the melting of synthetic H_2O-CO_2 fluid inclusions (− 56.6 °C), melting of ice and critical homogenization at 220 bar (374.1 °C) of synthetic H_2O inclusions in quartz. Reproducibility was ± 0.2 °C below 0 °C and ± 2 °C at the fluid inclusion homogenization temperatures (e.g., Navarro-Ciurana et al., 2016). A total of 224 inclusions were measured (Th + Tmi) by cycling down to − 180 °C and heating to the temperature of total homogenization to ensure stability of the inclusions and representativeness of the determinations. The cycling was generally repeated several times in order to avoid nucleation problems during freezing runs.

Homogenization of inclusions (Th) was by bubble disappearance (V?L). Salinities are expressed as wt.% NaCl equivalent and were estimated from the ice melting temperatures (*Tmi*) for two-phase fluid inclusions (e.g., Bodnar, 1993, Bodnar and Vityk, 1994). Due to the small inclusion sizes, no eutectic temperatures (*Te*) were measured. Salinity was estimated using the program *Aqso5e*, included in

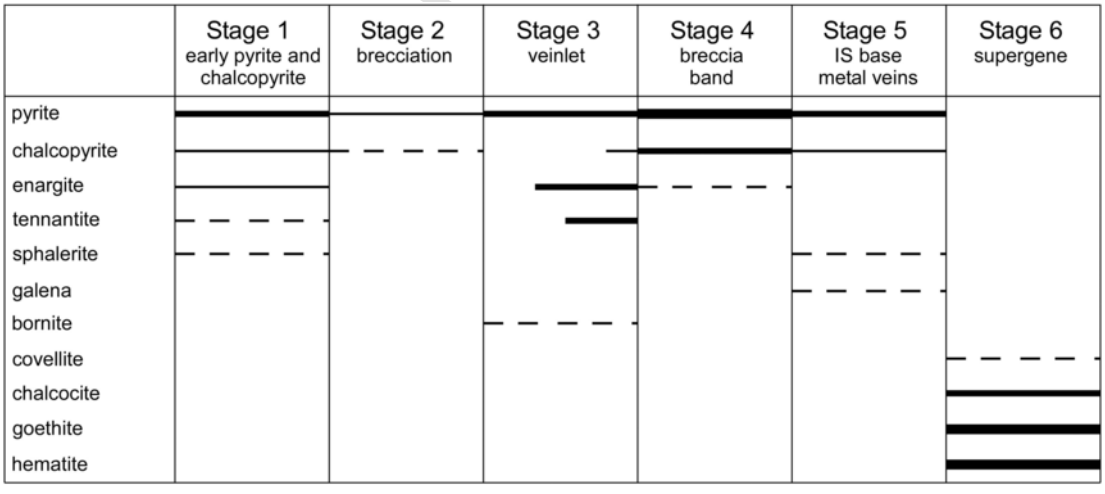

Fig. 5. Paragenetic sequence of ore minerals at Cerro Quema.

PROOF

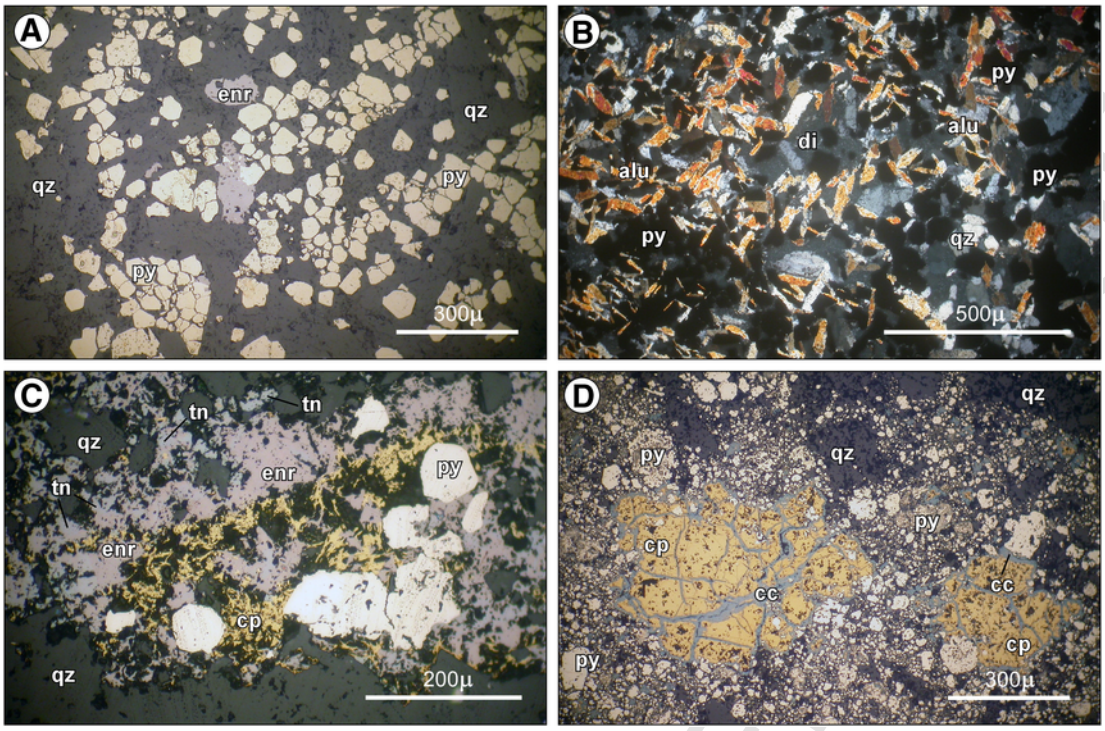

Fig. 6. Microscope images of alteration assemblages at Cerro Quema. A) Dissemination of pyrite and minor enargite in the vuggy quartz groundmass (stage 1). B) Alunite + pyrite ± dickite cemented hydraulic breccia (stage 2). C) Pyrite, chalcopyrite, enargite and tennantite veinlets (stage 3). Note the replacement textures of pyrite by enargite, enargite by tennantite and enargite-tennantite by chalcopyrite. D) Breccia band (stage 4) composed of pyrite, chalcopyrite, minor enargite and secondary copper-sulfides (chalcocite). Note the vuggy quartz altered clasts incorporated within the breccia band. All images are reflected polarized light, excepting B (transmitted crossed polarized light). alu: alunite, cc: chalcocite, cp: chalcopyrite, di: dickite, enr: enargite, py: pyrite, qz: quartz, tn: tennantite.

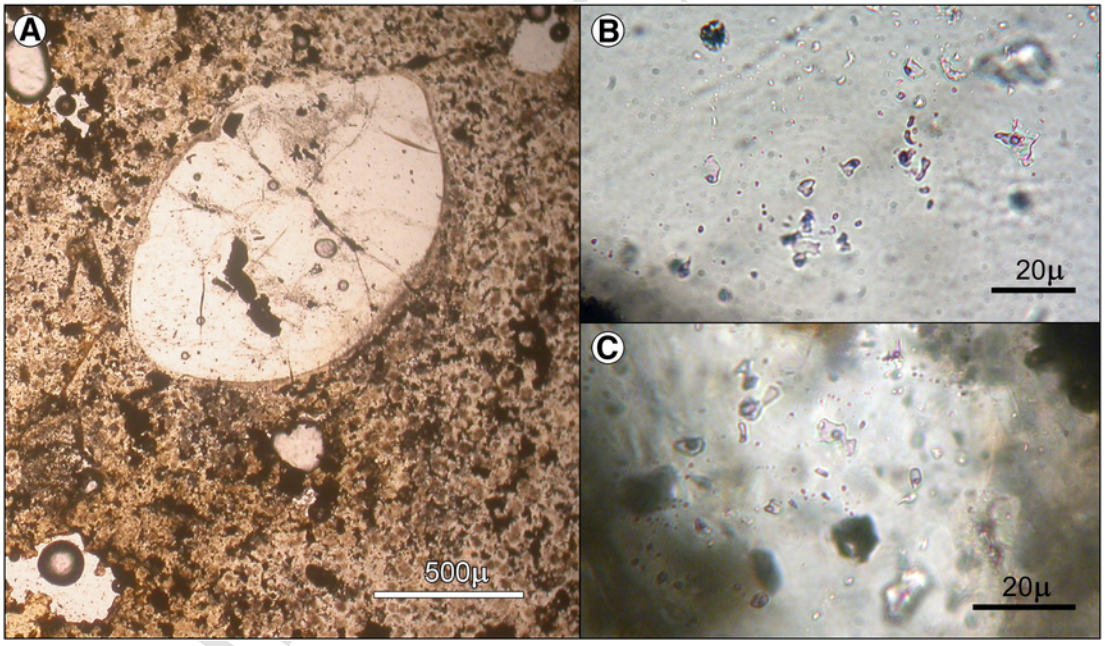

Fig. 7. Fluid inclusion types and occurrences. A) Igneous quartz phenocryst of a vuggy quartz altered dacite. B) Two-phase (L > V) fluid inclusion trails within a quartz phenocryst. C) Two-phase (L > V) fluid inclusions randomly distributed in a quartz phenocryst. All images are taken with transmitted polarized light.

the package FLUIDS (Bakker, 2003) following the equation of Potter *et al*. (1978), for NaCl bearing aqueous solutions of low temperature and low salinity.

4.2. Fluid inclusion types and occurrence

The fluid inclusion study was carried out on samples affected by different hydrothermal alteration types that are present throughout the deposit (Fig. 4): vuggy quartz from La Pava, Cerro Quemita, Chontal Edge and Cerro Idaida, and advanced argillic from Chontal Edge. Only one type of fluid inclusions was identified on the basis of the number of phases and liquid-to-vapor ratio at room temperature. These inclusions are two-phase (L + V) and are characterized by a dark vapor bubble generally less than 50% of the inclusion volume. They correspond to the two-phase liquid-rich (L > V) fluid inclusions described by Shepherd *et al*. (1985).

The inclusions show a variety of shapes: rounded, elongate or irregular, a few with negative crystal shapes (Fig. 7B and C). They are typically between 5 and 15 μm in diameter, which hampers observation of phase changes during heating-freezing runs. The studied fluid inclusions occur isolated, in clusters and following trails, all of them trapped in igneous quartz phenocrysts from the dacites of the Río Quema Formation (Fig. 7B). As fluid inclusions were trapped after the volcanic rock crystallization, during the later hydrothermal alteration, they are interpreted to be secondary in origin.

4.3. Microthermometrical data

The microthermometry results are summarized in Table 1 and Fig. 8. In general, heterogeneous trapping and postentrapment necking down are common features in inclusions from epithermal systems (Bodnar et al., 1985). We studied fluid inclusions in trails, groups and clusters where all inclusions showed similar liquid–vapor phase ratios as well as similar shape.

During the microthermometric measurements, phase transitions characteristic of the presence of volatiles (melting of CO_2 around − 56.6 °C or presence of CO_2 hydrates) were not observed, implying the absence of significant amounts of volatiles. However, some ice melting temperatures above 0 °C were observed (11 of 91 inclusions gave between 0.1 and 1.1 °C), which could indicate small quantities of CO_2 in the hydrothermal fluid. Calculated salinities should therefore be considered as maximum values, as CO_2 depresses the ice melting temperature (Hedenquist and Henley, 1985; Fall et al., 2011).

4.3.1. Vuggy quartz

Fluid inclusions in La Pava vuggy quartz sampled from outcrops (520 m above sea level; Fig. 8) have an average Th of 140 °C (σ = 10 °C) and an average Tmi of − 0.9 °C (σ = 0.6 °C). The calculated salinity is 1.6 wt% NaCl eq. Inclusions in La Pava vuggy quartz sampled from drill core (359 m above sea level; Fig. 8) have an average Th of 178 °C (σ = 11 °C) and an average Tmi of − 2.2 °C (σ = 0.5 °C), corresponding to a salinity of 3.7 wt% NaCl eq.

Vuggy quartz collected from Chontal Edge outcrops (334 m above sea level: Fig. 8) contains fluid inclusions with an average Th of 196 °C (σ = 19 °C). No Tmi measurements are available for this sample due to small inclusion size.

Further east, fluid inclusions of the vuggy quartz alteration zone from Cerro Quemita drill core (791 m above sea level; Fig. 8) are characterized by an average Th of 210 °C (σ = 17 °C). The average Tmi is − 0.3 °C (σ = 0.4 °C), equivalent to a salinity of 0.5 wt% NaCl eq.

In the easternmost part of the mineralized area, drill core samples of vuggy quartz from Cerrro Idaida (666 m above sea level; Fig. 8) are characterized by fluid inclusions with an average Th of 216 °C (σ = 46 °C). The average Tmi is − 2.9 °C (σ = 2.3 °C), equivalent to a salinity of 4.8 wt% NaCl eq.

Whether fluid temperature and salinity varied spatially during vuggy quartz alteration is difficult to determine unambiguously due to sparse data and high standard deviations for some Th and Tmi values. However, temperature increases are suggested from surface to depth in the La Pava deposit and from west to east from La Pava to Cerro Idaida.

4.3.2. Advanced argillic

The scarcity of secondary fluid inclusions in igneous quartz phenocrysts precluded a better systematic study for the advanced argillic alteration-forming fluids. Only one drill core sample from the Chontal Edge could be studied (341 m above sea level, Fig. 8). Fluid inclusions from this sample have an average Th of 205 °C (σ = 11 °C), and an average Tmi of − 1.4 °C (σ = 0.8 °C), which corresponds to a salinity of 2.4 wt% NaCl eq.

5. Stable Isotopes

5.1. Sampling and analytical methods

Stable isotope analyses (O, H and S) were carried out on 65 surface and drill core samples from the Cerro Quema deposit at the laboratories of the USGS Crustal Geophysics and Geochemistry Science Center in Denver (USA). Pyrite, chalcopyrite, enargite, barite, vuggy quartz and igneous quartz phenocrysts were handpicked from crushed and sieved samples. Kaolinite, dickite and alunite were separated by decantation methods to obtain the clay fraction and then by centrifugation to separate the different minerals. Mineral separates were checked by X-ray diffraction to assure purity. Identification of the different clay minerals was performed by oriented X-ray diffraction.

Sulfates and sulfides were combined with V_2O_5 and combusted in an elemental analyzer, the resulting SO_2 flowed directly into a Thermo Delta mass spectrometer for sulfur isotope measurement ($\delta^{34}S$) according to the method of Giesemann *et al*. (1994), with a precision of ± 0.5‰ (2σ). Oxygen isotope analyses of sulfates were

Table 1
Summary of microthermometric results for fluid inclusions of the Cerro Quema deposit. All measurements were performed in quartz phenocrysts (see text for explanation). AAA: advanced argillic alteration, Th: homogenization temperature, Tmi: melting ice temperature, VQ: vuggy quartz alteration.

Sample	Deposit	Alteration Zone	Coordinates (°WGS84)		Elevation (asl)	Th (°C) range (N)	Th avgerage	Tmi (°C) range (N)	Tmi avgerage	wt% NaCl eq.
			longitude	latitude						
LP05	La Pava	VQ	7.552843	-80.545937	520 m	123.3–156.4 (21)	140 °C ± 10	-1.5 to − 0.3 (5)	-0.9 °C ± 0.6	1.6
9311	La Pava	VQ	7.553654	-80.548764	359 m	160.2–199.1 (20)	178 °C ± 11	-3.3 to − 1.3 (18)	-2.2 °C ± 0.5	3.7
0608	Chontal Edge	VQ	7.554922	-80.537961	297 m	170.9–227.7 (16)	196 °C ± 19	–	–	–
9104	Cerro Quemita	VQ	7.560327	-80.519231	791 m	181.2–238.3 (22)	210 °C ± 17	-1.3 to 0.0 (16)	-0.3 °C ± 0.4	0.5
9343	Cerro Idaida	VQ	7.555226	-80.507060	666 m	147.5–310.0 (24)	216 °C ± 46	-7.8 to − 0.6 (20)	-2.9 °C ± 2.3	4.8
0308	Chontal Edge	AAA	7.557230	-80.534429	341 m	183.4–226.3 (30)	205 °C ± 11	-3.3 to − 0.1 (21)	-1.4 °C ± 0.8	2.4

UNCORRECTED PROOF

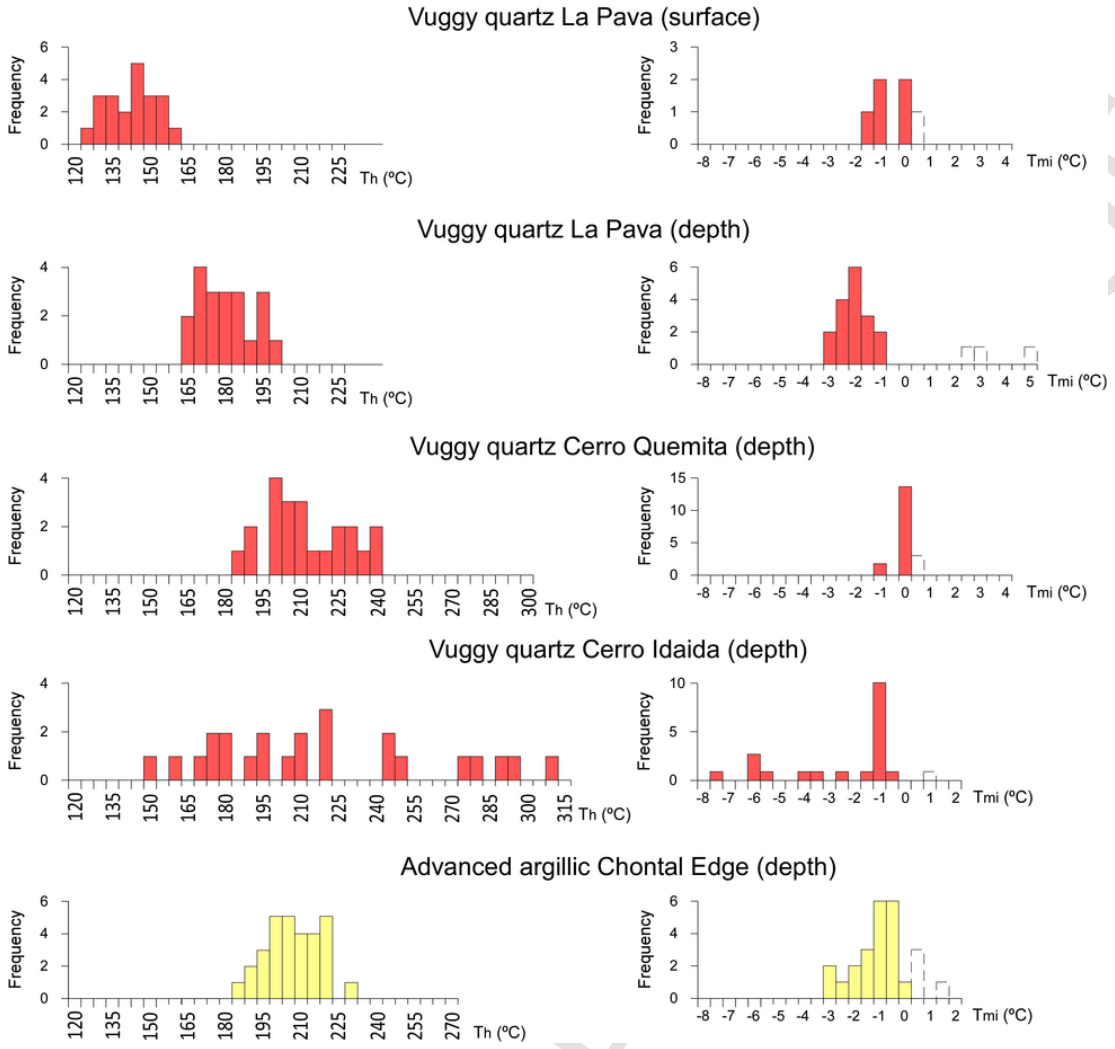

Fig. 8. Fluid inclusion frequency histograms. Homogenization temperature (*Th*) and melting ice temperature (*Tmi*) of Cerro Quema fluid inclusions. Discontinue line represent fluid inclusions that melted above 0 °C.

performed by online high-temperature carbon reduction, with a precision of ± 0.6‰ (2σ). Silicates were reacted with BrF_5 (Clayton and Mayeda, 1963) and the resulting CO_2 gas was analyzed using a FinniganMAT252 mass spectrometer, with a precision of ± 0.3‰ (2σ) for $\delta^{18}O$. H isotope ratios of kaolinite-dickite were determined with a FinniganMAT252 mass spectrometer, using the method of Vennemann and O'Neil (1993), with a precision of ± 2‰ (2σ) for δD. Analytical precision was based on replicate analyses. The $\delta^{18}O$ and δD analyses are reported in per mil values relative to V-SMOW, and the $\delta^{34}S$ values are reported relative to the Vienna Cañon Diablo Troilite standard.

5.2. Sulfur isotopes

Sulfur isotope data were obtained on pyrite ($n = 22$), enargite ($n = 8$), chalcopyrite ($n = 1$), barite ($n = 5$) and alunite ($n = 6$), (Table 2 and Fig. 9). The range of $\delta^{34}S$ of sulfides is from − 4.8 to − 12.7‰, whereas $\delta^{34}S$ of sulfates range from 14.1 to 17.4‰. The $\delta^{34}S$ values of sulfides and sulfates are similar to those reported in other high sulfidation epithermal deposits such as Summitville, USA (Rye et al., 1990, 1992; Bethke et al., 2005), Lepanto Phillipines (Hedenquist and Garcia, 1990) and Pueblo Viejo, Dominican Republic (Kesler et al., 1981; Vennemann et al., 1993). Comparing the sulfur composition of sulfides and sulfates in the different orebodies of the Cerro Quema deposit reveals no significant variability, suggesting a homogeneous sulfur source at deposit scale.

5.3. Oxygen and hydrogen isotopes

Oxygen isotope analyses were performed on vuggy quartz ($n = 24$), kaolinite ($n = 19$) dickite ($n = 4$), alunite (n = 6), barite (n = 5) and igneous quartz phenocrysts ($n = 3$). Hydrogen isotope analysis were performed on kaolinite (n = 19) and dickite (n = 4). Results are shown in Table 2.

The $\delta^{18}O$ values of vuggy quartz (9.0 to 17.5‰) are higher than those of quartz phenocrysts of the Cerro Quema host dacite (8.6 to 8.8‰). In general, igneous quartz phenocrysts in altered rocks retain their primary isotopic compositions (Taylor, 1968; Fifarek and Rye, 2005). This is shown by igneous quartz phenocryst composition of samples QA32 and LP218 (vuggy quartz altered; Table 2), and igneous quartz phenocryst composition of sample LP204 (fresh dacite; Table 2). Therefore, acid leaching and vuggy quartz alteration resulted in a ~ 0.5 to 8.9‰ $\delta^{18}O$ enrichment of the microcrystalline

Table 2
Summary of the stable isotope data (S, O, H) from the different minerals analyzed in this study. al: alunite, ba: barite, cpy: chalcopyrite, en: enargite, kaol-dck: kaolinite-dickite, py: pyrite.

Sample	$\delta^{18}O$ (ba)	$\delta^{34}S$ (ba)	$\delta^{18}O$ (al)	$\delta^{34}S$ (al)	$\delta^{34}S$ (py)	$\delta^{34}S$ (en)	$\delta^{34}S$ (cpy)	δD (Kaol-dck)	$\delta^{18}O$ (Kaol-dck)	$\delta^{18}O$ (quartz)
Chontal edge										
0308–29.6								-30	14.6	
0308–51.80			9.8	17.4	-8.2					10.4
0308–60.40			6.7	15.6	-8.2					
0308–60.40			6.6		-8.4					
0308–65.80					-8.3	-9.3		-44	12.7	
0308–73.6					-8.0					
0308–95.50			4.2	17.3	-8.5					9.0
0308–98.35					-7.2	-11.2				
0308–104.15			-1.6	17.2	-8.4					10.7
0308–104.15				17.2						
0308–105.50					-11.7			-39	12.7	
0308–111.60			4.9	15.0	-7.2	-12.1				
0308–111.60					-7.2					
0308–131.10								-36	16.3	
0308–134.15					-9.0					
QUE 51	15.5				-4.8		-5.5			16.6
QUE 51	16.2				-5.2					13.5
QUE Kan	10.8	15.4								
QUE Kan	10.8	15.5								
La Pava										
9316–182	11.6	16.9								
9316–190	10.9	17.1								
LP216								-66	17.1	
LP04								-47	17.9	
LP212A								-46	17.6	
LP226								-80	15.6	
LP226								-81	15.6	
LP225					-12.7					
LP225					-12.6					
LP223								-42	15.5	
LP228								-57	18.1	
LP215								-77	16.6	
LP211								-41	15.2	
LP213B								-35	17.7	
LP213B								-36	17.7	
LP222								-40	15.4	
CLP4								-38	16.9	
CLP4								-42	16.9	
LP218										17.5
LP220										16.6
9210–16					-7.6					16.2
9322–78										15.5
9311–106										12.9
9311–153										12.5
Cerro Quemita and Cerro Quema										
QT02	2.7	14.1								
QA05								-103	14.3	
QA15A								-50	17.4	
QA30								-48	17.1	
QA29								-52	17.4	
QA24								-39	18.0	
QA10										12.9
QA17B										11.8
QA32										12.3
914–59										11.7
914–82										12.5
9315–130					-10.7					12.1
Cerro Idaida										
9343–36					-12.1	-7.5				13.7
9325–56					-6.7	-7.9				11.9
9325–56					-6.0	-8.6				
9343–66						-5.3				11.4
9343–66						-5.0				
Pyrite El Montuoso bathoith										
Pit-01					3.3					
Quartz Valle Rico batholith										
Tri-01										3.6

UNCORRECTED PROOF

Table 2 (*Continued*)

Sample	$\delta^{18}O$ (ba)	$\delta^{34}S$ (ba)	$\delta^{18}O$ (al)	$\delta^{34}S$ (al)	$\delta^{34}S$ (py)	$\delta^{34}S$ (en)	$\delta^{34}S$ (cpy)	δD (Kaol-dck)	$\delta^{18}O$ (Kaol-dck)	$\delta^{18}O$ (quartz)
Quartz phenocrystals Dacite dome complex (RQF)										
LP218										8.8
LP204										8.7
QA32										8.6

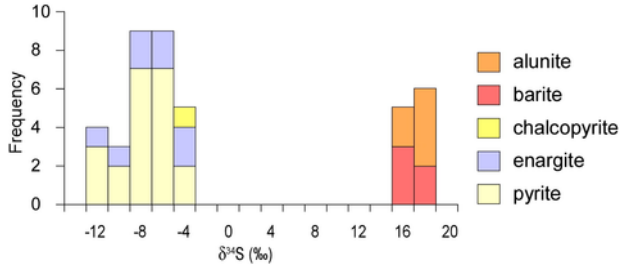

Fig. 9. $\delta^{34}S$ frequency histogram of sulfides and sulfates of Cerro Quema.

quartz with respect to the igneous quartz phenocrysts (e.g., sample LP218: 17.5‰ and 8.8‰, respectively; Table 2). The $\delta^{18}O$ values of vuggy quartz show a wide variability throughout the Cerro Quema deposit. They become higher from east to west in surface samples (11.8% at Cerro Quema to 17.5% at La Pava) and lower from surface to depth (17.5% at La Pava surface to 12.5% at La Pava at depth).

The $\delta^{18}O$ values of kaolinite range from 12.7 to 18.1‰ and δD from − 103 to − 35‰, whereas $\delta^{18}O$ of dickite varies between 12.7 and 16.3‰ and δD from − 44 to − 30‰. Although δD values of kaolinite and dickite are highly variable in the Cerro Quema deposit, $\delta^{18}O$ values, show a trend from higher values in the east to lower values in the west (from 18‰ at Cerro Quema to 16‰ at La Pava), in agreement with $\delta^{18}O$ values of vuggy quartz. Alunite and barite show a wide $\delta^{18}O$ range, with alunite varying from − 1.6 to 9.8‰, and barite ranging from 2.7 to 11.6‰.

6. Discussion

6.1. Characteristics of the hydrothermal fluid

In studying any hydrothermal system it is essential to determine the thermal history, as this relates to fluid flow characteristics and geochemical structure (Hedenquist et al., 1992). Two of the principal physical processes occurring in the epithermal environment are boiling and mixing (Giggenbach and Stewart, 1982). Fluid inclusion data (*Th* and *Tmi*) provide information on these processes at Cerro Quema.

Results of microthermometric measurements on secondary fluid inclusions from the Cerro Quema deposit are shown on a *Tmi* vs. *Th* plot in Fig. 10. The relationship between homogenization and melting ice temperatures is complicated, probably reflecting a complex sequence of fluid events. Only the study of individual samples or a group of samples with the same characteristics helps to understand the processes recorded by the fluid inclusions.

When fluid inclusions of the advanced argillic alteration zone (Chontal Edge) and of the vuggy quartz (La Pava surface and depth) are plotted together (Fig. 10A), a trend evolving from high *Tmi* and low *Th* towards low *Tmi* and high *Th* can be recognized. The most likely interpretation is that they represent a heterogeneous fluid resulting from isothermal mixing of fluids with different origins (e.g., Wilkinson, 2001; Morales-Ruano et al., 2002). However, they can also be interpreted as indicative of a boiling process with slight cooling (Sheppard et al., 1985; Hedenquist and Henley, 1985), although no evidence of boiling were observed in the petrography study.

On the other hand, in Fig. 10B, where fluid inclusions of the vuggy quartz (Cerro Idaida and Cerro Quemita at depth) are plotted,

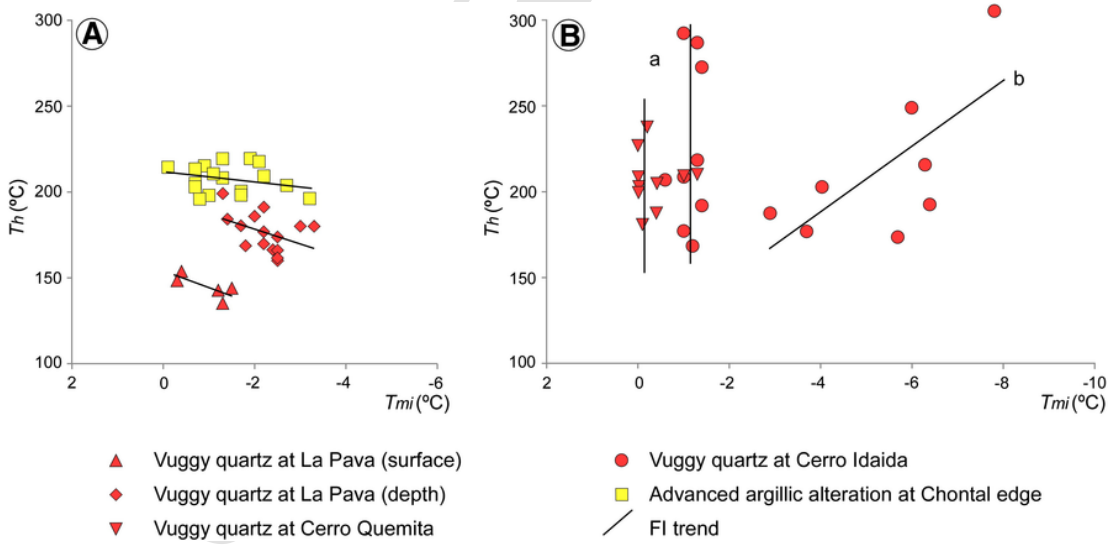

Fig. 10. Homogenization temperature (*Th*) – Melting ice temperature (*Tmi*) plots. A) *Th-Tmi* plot showing fluid inclusion data of vuggy quartz altered dacites form La Pava (surface and drill core), and of advanced argillic altered dacite at Chontal Edge. B) *Th-Tmi* plot showing fluid inclusion data of vuggy quartz altered dacites from Cerro Quemita and Cerro Idaida.

CORRECTED PROOF

two different trends can be distinguished. A first trend is characterized by fluid inclusions with uniform *Tmi* and variable *Th* (a).The second trend is characterized by fluid inclusions with high *Tmi* and high *Th* evolving towards low *Tmi* and low *Th* (b). According to Sheppard *et al*. (1985) and Hedenquist and Henley (1985), these trends would be indicative of simple cooling and mixing or dilution of the fluid with cooler and a less saline fluid, respectively. Such processes could explain the high standard deviation (σ) observed in some of the Cerro Quema fluid inclusion data (*Th* and *Tmi*).

On the basis of fluid inclusion data, the hydrothermal fluids at Cerro Quema varied from 140 to 212 °C, and had low salinity (from 0.5 to 4.3 wt% NaCl). *Th* vs. *Tmi* plots (Fig. 10) clearly suggest processes such as mixing of magmatic and meteoric fluids. These processes have been documented in several other high sulfidation deposits (e.g., Arribas, 1995).

6.2. Sulfur source and geothermometry

The isotopic composition and evolution of total sulfur ($\delta^{34}S_{\Sigma S}$) in a hydrothermal fluid may provide insights as to the provenance of sulfur and the conditions of mineral formation. Coexisting sulfides and sulfates may, in turn, be useful for sulfur isotope thermometry. Alunite is an important mineral component of the advanced argillic alteration assemblage and is abundant in drill core samples from the Chontal Edge. Textural and mineralogical relationships indicate that alunite was contemporaneous with associated pyrite.

According to Field and Gustafson (1976), Kusakabe *et al*. (1984) and Field et al. (1983, 2005), the use of $\delta^{34}S$ of sulfide and sulfate vs. $\Delta^{34}S_{\text{sulfate-sulfide}}$ plot is a powerful tool to estimate the $\delta^{34}S_{\Sigma S}$, XSO_4^{2-} and XH_2S of the hydrothermal fluid (assuming isotopic equilibrium between sulfate and sulfide). The $\delta^{34}S$ of coexisting pyrite and alunite from Chontal Edge (Table 2) are shown in a $\delta^{34}S$-$\Delta^{34}S_{\text{sulfate-sulfide}}$ plot in Fig. 11A. Linear regression of alunite-pyrite pairs indicates two converging trends; the point of convergence of these two lines on the *y* axis ($\delta^{34}S$) defines the value for $\delta^{34}S_{\Sigma S}$, whereas the slopes of the upper and lower regression lines approximate the XSO_4^{2-} and XH_2S of the system, respectively.

Based on Fig. 11A, the $\delta^{34}S_{\Sigma S}$ value of the hydrothermal fluid responsible for the Cerro Quema deposit is − 0.5‰, and calculated XSO_4^{2-} and XH_2S are 0.3 and 0.7 respectively, with a H_2S/SO_4^{2-} (R) ratio of 2.2. These results suggest that: 1) sulfur in the deposit is of magmatic origin, with a $\delta^{34}S_{\Sigma S}$ value similar to that reported in other high sulfidation epithermal deposits and porphyry copper deposits associated with I-type granites (Ohmoto and Goldhaber, 1997; Hedenquist and Lowenstern, 1994; Arribas, 1995); 2) fluids responsible for the pyrite and alunite alteration assemblages have R value that is in the range of hydrothermal ore-forming fluids (4 ± 2; Rye et al., 1992; Hedenquist et al., 1994; Arribas et al., 1995; Arribas, 1995); 3) the magmatic-hydrothermal system at Cerro Quema was produced by a sulfide dominant hydrothermal fluid.

Comparison of the sulfur isotope composition of sulfides and sulfates in the different ore bodies of Cerro Quema reveals no significant variability, suggesting that the sulfur source was homogeneous at the deposit scale. $\delta^{34}S$ values of sulfides coexisting with sulfates reflect isotopic equilibrium between H_2S and SO_4^{2-} in the hydrothermal fluid (Fig. 9). Equilibrium among these species is typical of magmatic-hydrothermal deposits (Rye, 2005), and has been observed in world class high sulfidation epithermal deposits (e.g., Field and Fifarek, 1985; Arribas, 1995). Using the equation of Rye et al., (1982), calculated equilibrium temperatures for alunite-pyrite pairs range between 221 and 271 °C (*n* = *6*; Fig. 11B). The average equilibrium temperature is 239 °C (σ = 20), which is slightly higher than the *Th* values measured in the advanced argillic alteration fluid inclusions (205 ± 11 °C).

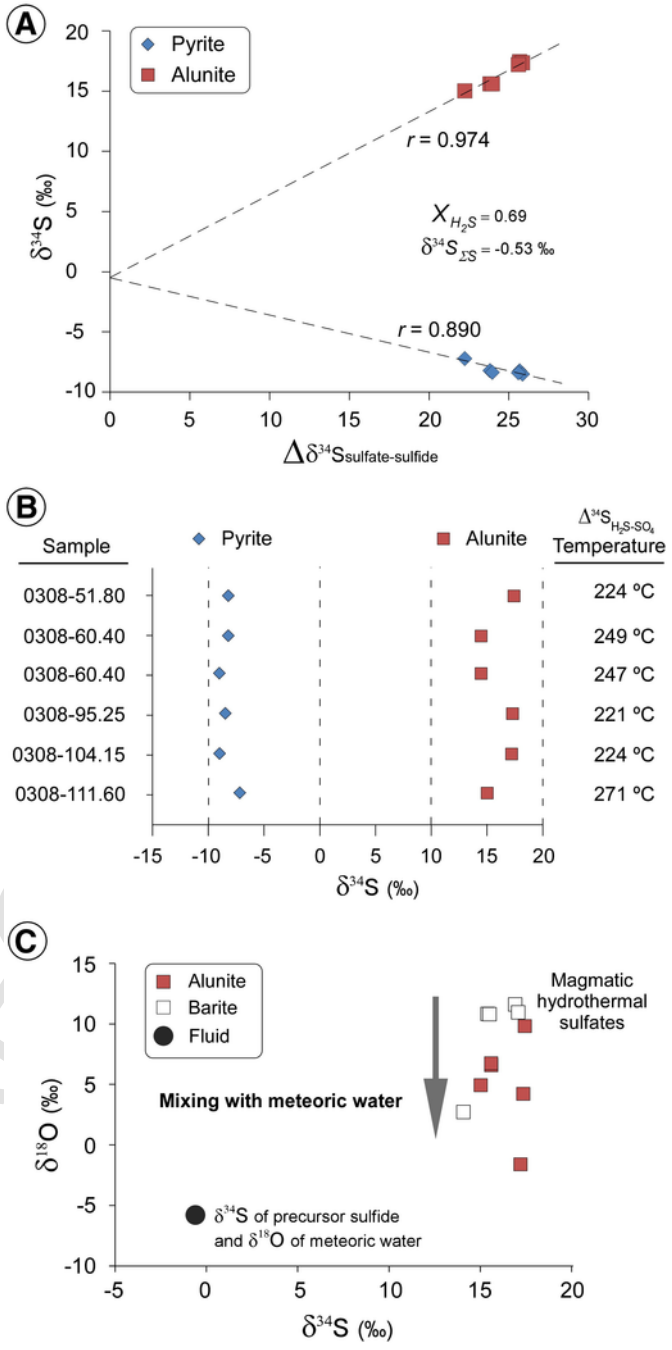

Fig. 11. Summary of $\delta^{34}S$ and $\delta^{18}O$ data on alunite, barite and pyrite. A) $\delta^{34}S$ plot of sulfate (alunite) and sulfide (pyrite) pairs vs. delta (Δ) value. The convergence and slope of the two regression lines is an approximation of the bulk sulfur isotopic composition ($\delta^{34}S_{\Sigma S}$) and the proportion of oxidized to reduced sulfur species (XSO_4^{2-} and XH_2S) in the hydrothermal fluid (see text for explanation). B) $\delta^{34}S$ values of sulfides and sulfates from the advanced argillic alteration zone. The temperature determined from sulfide-sulfate mineral pairs is also shown. C) $\delta^{34}S$ and $\delta^{18}O$ of barite and alunite showing a vertical trend, indicating a mixing between magmatic sulfate and meteoric waters (see text for explanation).

This difference may be due to the pressure effect on the trapping temperatures of the fluids during the advanced argillic alteration

event. Sulfur isotope temperatures are consistent with the disproportionation temperature of magmatic SO_2 to $H_2S + SO_4^{2-}$ in the hydrothermal solution, which is known to be below 400 °C (Sakai and Matsubaya, 1977; Bethke, 1984; Stoffregen, 1987; Rye et al., 1992).

6.3. $\delta^{34}S$ / $\delta^{18}O$ of alunite and barite

$\delta^{34}S$ and $\delta^{18}OSO_4^{2-}$ values of alunite and barite from the advanced argillic alteration zone at Cerro Quema are shown in Fig. 11C. Both minerals present a narrow range of $\delta^{34}S$ values (14.1 to 17.4‰), but variable $\delta^{18}O$ values, ranging from − 1.6 to 11.6‰. According to these isotopic characteristics, the Cerro Quema sulfates fall within the magmatic-hydrothermal field defined by Rye *et al*. (1992) and Rye (2005). The relatively high $\delta^{34}S$ values are consistent with sulfate derivation from sulfuric acid produced by disproportionation of magmatic SO_2, which reacted with the wall rocks to produce the acid-sulfate alteration (Holland, 1965; Stoffregen, 1987). However, the variable $\delta^{18}O$ values, which define the vertical trend of the data, suggest that disproportionation may have occurred in mixtures of magmatic and meteoric waters, typically as the result of condensation of magmatic steam in meteoric groundwaters. The effect of mixing between magmatic and meteoric waters is to decrease the $\delta^{18}O$ by an amount dependent on the $\delta^{18}O$ and the degree of involvement of meteoric waters (Rye et al., 1992). This interpretation is in agreement with the microthermometry data obtained from fluid inclusions in the vuggy quartz and the advanced argillic alteration zone, which suggest mixing with cooler and less saline fluids (e.g., meteoric waters).

6.4. H and O isotope composition of hydrothermal fluids

Studies of fluid-mineral isotopic equilibrium in geothermal systems have shown that quartz is very resistant to isotopic exchange, preserving the original isotopic signature (Clayton et al., 1968; Taylor, 1968; Blattner, 1975; Clayton and Steiner, 1975; Fifarek and Rye, 2005). If the hydrothermal fluids had uniform oxygen isotopic composition, the increase in $\delta^{18}O$ would reflect decreasing temperatures of mineral precipitation, which is in agreement with the decrease in the homogenization temperatures obtained from fluid inclusions.

Also, $\delta^{18}O$ values of vuggy quartz decrease with depth, suggesting an increase in temperature towards the deeper parts of the system, a characteristic of other high sulfidation epithermal deposits such as Summitville, USA (Larson and Taylor, 1987; Bethke et al., 2005). Thus, the $\delta^{18}O$ values of vuggy quartz may be useful as an exploration vector in high sulfidation deposits and lithocaps indicating the direction of hotter conditions closer to the fluid source, presumably indicating the direction of a causative porphyry intrusion that may represent a target for Cu mineralization.

As shown in Fig. 12, the $\delta^{18}O$ values of vuggy quartz at Cerro Quema, overlap those from other high sulfidation epithermal deposits such as Summitville (USA; Larson and Taylor, 1987; Bethke et al., 2005), Pueblo Viejo (Dominican Republic; Vennemann et al., 1993), Pierina (Peru; Fifarek and Rye, 2005), Nansatsu (Japan; Hedenquist et al., 1994) and Rodalquilar (Spain; Arribas et al., 1995).

Using temperatures of quartz formation from the of fluid inclusion data; 160 °C for La Pava (surface-depth average), 205 °C for Chontal Edge, 210 °C for Cerro Quemita, 212 °C for Cerro Quema, and 212 °C for Cerro Idaida, the calculated $\delta^{18}O$ values of the vuggy quartz-forming fluid ranges from − 2.3 to 3.0‰ (quartz–water fractionation of Matsuhisa et al., 1979). These values plot between arc type magmatic water $\delta^{18}O$ values (Taylor, 1986; Giggenbach, 1992)

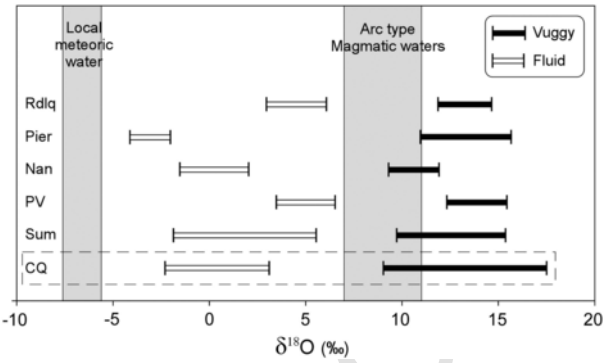

Fig. 12. Diagram showing the range of vuggy quartz $\delta^{18}O$ values and $\delta^{18}O$ values of vuggy quartz-froming fluids. For comparison data from Rodalquilar (Arribas et al., 1995), Pierina (Fifarek and Rye, 2005), Nansatsu (Hedenquist et al., 1994), Pueblo Viejo (Vennemann et al., 1993), and Summitville (Larson and Taylor, 1987; Bethke et al., 2005) has been represented. Local meteoric waters field from Caballero (2010); arc type magmatic waters field from Taylor (1986) and Giggenbach (1992). Rdl: Rodalquilar, Pier: Pierina, Nan: Nansatsu, PV: Pueblo Viejo, Sum: Summitville.

and present day meteoric water $\delta^{18}O$ values (Caballero, 2010). Thus, Cerro Quema vuggy quartz probably precipitated from magmatic fluids diluted by variable amounts of meteoric water.

Kaolinite and dickite are widespread within the argillic and advanced argillic alteration zones at Cerro Quema. The isotopic compositions of these minerals ($\delta^{18}O$ and δD) may reflect the geological conditions during the mineral deposition (e.g., Savin and Lee, 1988). For instance, $\delta^{18}O$ values of kaolinite of sedimentary origin usually vary from 19 to 23‰, whereas those of kaolinite from residual deposits (primary) range from 15 to 19‰ (Murray and Janssen, 1984). $\delta^{18}O$ and δD values of dickite and kaolinite from Cerro Quema range from 12.7 to 18.1‰, and from − 30 to − 103‰, respectively, and are shown in Table 2 and plotted in Fig. 13.

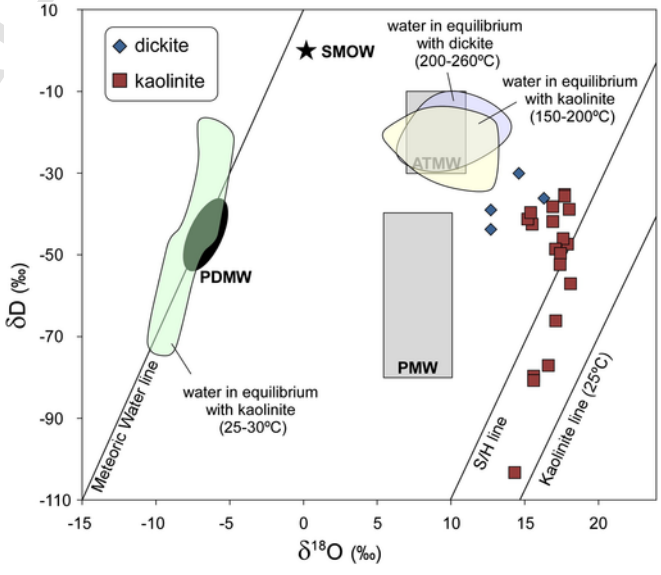

Fig. 13. Plot of $\delta^{18}O$ and δD values of kaolinite and dickite, and the values of water in equilibrium with them. PDMW: Present day meteoric water (Caballero, 2010), PMW: Primary magmatic waters (Taylor, 1974; Sheppard, 1986), ATMW: Arc-type magmatic waters (Taylor, 1986; Giggenbach, 1992), S/H line: Supergene/Hypogene line (Sheppard et al., 1969), Kaolinite line (25 °C; Savin and Epstein, 1970; Sheppard and Gilg, 1996).

UNCORRECTED PROOF

On the basis of mineralogy and $\delta^{18}O/\delta D$ relations, two populations of kaolinite-group minerals can be distinguished (Fig. 13). One group lies between the supergene/hypogene line (S/H; Sheppard et al., 1969), and the 25 °C kaolinite line (Savin and Epstein, 1970; Sheppard and Gilg, 1996), corresponding to kaolinites of supergene origin. A second group plots between the S/H line and the Arc Type Magmatic Waters box and are considered to be of hydrothermal origin.

At Cerro Quema kaolinite occurred in argillically altered rocks with little presence of primary sulfides and similar oxidation overprint. No distinction could be made with petrographic observations and X-ray diffraction analysis. In this case, isotope $\delta^{18}O/\delta D$ values composition seems to be the best way to distinguish between meteoric and hydrothermal kaolinites.

In order to estimate the isotopic composition of fluids responsible for the kaolinite and dickite precipitation, a temperature range based on fluid inclusion data, mineral paragenesis and isotope geothermometry was used. The assumed temperatures were: 200 to 260 °C for dickites, 150 to 200 °C for hypogene kaolinites, and 25 to 30 °C for kaolinites of supergene origin. Calculations have been performed using the fractionation equations of Gilg and Sheppard (1996), and Sheppard and Gilg (1996) for oxygen and hydrogen, respectively.

The results (Fig. 13) show fluid δD and $\delta^{18}O$ values corresponding to dickite of − 28 to − 13‰ and 7.1 to 13.3‰, respectively. Fluid δD and $\delta^{18}O$ values corresponding to hypogene kaolinite range from − 32 to − 15‰ and 6.5 to 12.4‰, respectively. These ranges are compatible with an origin related to the arc-type magmatic waters defined by Taylor (1986) and Giggenbach (1992).

On the other hand, fluid δD and $\delta^{18}O$ values corresponding to supergene kaolinite range from − 72 to − 20‰ and − 10.0 to − 5.2‰, respectively (Fig. 13). These results imply formation of supergene kaolinite from water with an isotopic composition similar to present-day meteoric water (PDMW; Caballero, 2010).

7. Conclusions

The findings of the previous discussion are summarized in this section and illustrated in Fig. 14, which illustrates our interpretation of the magmatic-hydrothermal system at Cerro Quema. From the perspective of stable isotope geochemistry (O, H, and S) and fluid inclusion microthermometry, the main conclusions are as follows:

1) Fluid inclusion data reveal a hydrothermal fluid of low temperature (140–216 °C) and low salinity (0.5–4.8 wt% NaCl eq.). The fluid was cooler in the western La Pava area and hotter in the eastern Cerro Quema and Cerro Idaida areas, suggesting that the eastern part of the deposit is more proximal to the fluid and heat source.
2) The fluid in the magmatic-hydrothermal system was sulfide dominant ($XH_2S = 0.69$) and the sulfur was of magmatic origin ($\delta^{34}S_{\Sigma S} = -0.5‰$). However, variable $\delta^{18}O$ at constant $\delta^{34}S$ of alunite and barite, and $\delta^{18}O$ values of fluids in equilibrium with vuggy quartz (− 2.3–3.1‰), suggest dilution of magmatic fluid by meteoric waters (e.g., groundwater) during alteration/mineralization.
3) Alunite-pyrite sulfur isotope geothermometry indicates average equilibration temperatures of 239 °C (σ = 20) for the advanced

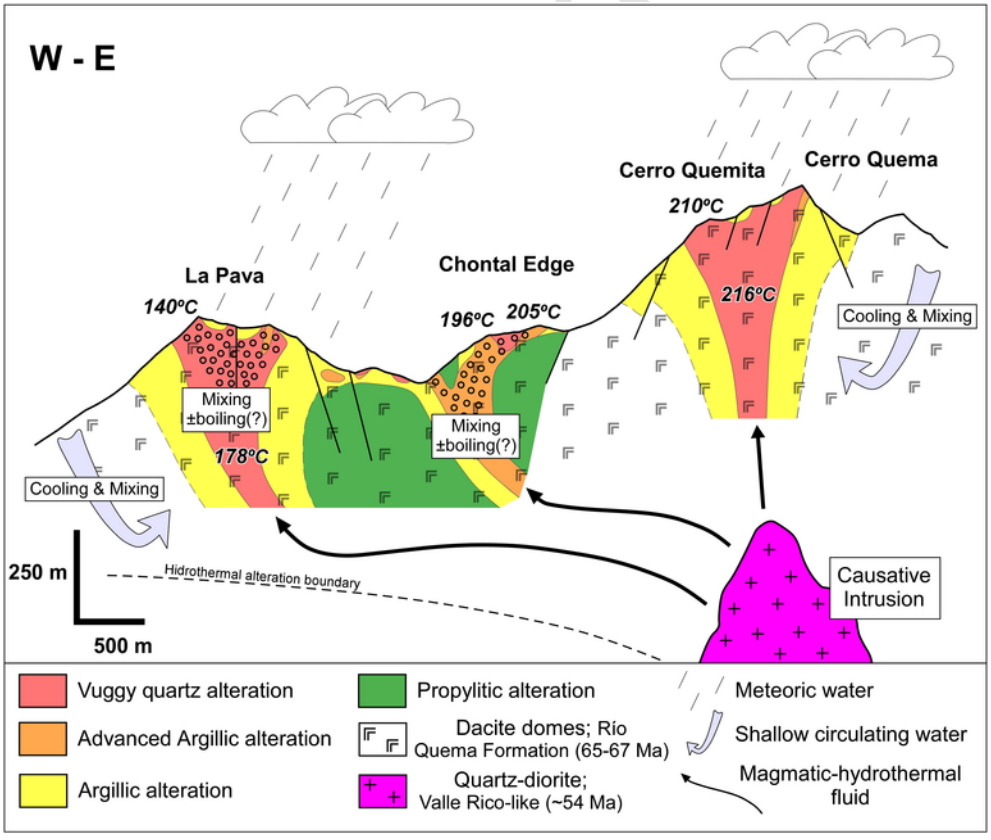

Fig. 14. Conceptual model of Cerro Quema hydrothermal system integrating the fluid inclusion (temperatures) and the stable isotope (processes) interpretations. Microthermometric and geochemical data presented in this work suggest the location of a causative porphyry copper-like intrusion towards the east of the deposit at certain depth.

argillic alteration, slightly higher than fluid inclusion measured in the same hydrothermal alteration, 205 °C (σ = 11).

4) $\delta^{18}O$ values of vuggy quartz decrease from western La Pava area to the eastern Cerro Quema area and from surface to depth. This reflects progressively lower temperatures of deposition and suggests that the fluid and heat source was situated to the east of the Cerro Quema deposit and at depth.
5) Cerro Quema is a high sulfidation epithermal Au-Cu deposit generated by the interaction of surface waters with fluids derived from a porphyry copper-like intrusion at depth to the east of the deposit.
6) The combination of fluid inclusion and stable isotope data at Cerro Quema provide vectors for exploration of porphyry Cu-Au deposits which may be applicable elsewhere.

Acknowledgments

This study is part of the first author's Ph.D., performed within the framework of the Ph.D. program in Geology of the Universitat Autònoma de Barcelona. The research was supported through the research project CGL2007–62,690/BTE (Spanish Ministry of Science and Education), and a by a predoctoral grant from the "Departament d'Universitats, Recerca i Societat de la Informació (Generalitat de Catalunya)". The corresponding author would like to express his gratitude to the SEG Foundation and the SEG Canada Foundation for the 2009, 2010 and 2011 Hugh E. McKinstry student research grants, which paid for part of the field and related laboratory research expenses. We thank Bellhaven Copper and Gold Inc. for access to mine samples and drill cores used in this study. We really appreciate help and support of Cayce A Gulbransen and George Breit in the understanding of the stable isotope analytical techniques and alunite separation/analytical techniques respectively. We also thank the helpful comments by Ryan Taylor (USGS reviewer) on the final manuscript draft. The manuscript significantly benefited from a thorough review and many constructive comments by Dr. Antonio Arribas and anonymous reviewer. Any use of trade, product, or firm names is for descriptive purposes only and does not imply endorsement by the U.S. Government.

References

Arribas, A., 1995. Characteristics of high-sulfidation epithermal deposits, and their relation to magmatic fluid. In: Thompson, J.F.H. (Ed.), Magmas, Fluids, and Ore Deposits. Mineral. Assoc. Can. Short Course, vol. 23, pp. 419–454.

Arribas, A., Cunningham, C.G., Rytuba, J.J., Rye, R.O., Kelly, W.C., Podwysocky, M.H., McKee, E.H., Tosdal, R.M., 1995. Geology, geochronology, fluid inclusions, and isotope geochemistry of the Rodalquilar gold alunite deposit, Spain. Econ. Geol. 90, 795–822.

Bakker, R.J., 2003. Package FLUIDS 1. Computer programs for analysis of fluid inclusion data and for modelling bulk fluid properties. Chem. Geol. 194, 3–23.

Bethke, P.M., 1984. Controls on base- and precious-metal mineralization in deeper epithermal environments. In: U.S. Geol. Surv. Open-File Rep. pp. 84–890.

Bethke, P.M., Rye, R.O., Stoffregen, R.E., Vikre, P.G., 2005. Evolution of the magmatic-hydrothermal acid-sulfate system at Summitville, Colorado; integration of geological, stable isotope, and fluid inclusion evidence. Chem. Geol. 215, 281–315.

Blattner, P., 1975. Oxygen Isotopic composition of fissure-grown quartz, adularia, and calcite from Broadlands geothermal field, New Zealand. Am. J. Sci. 275, 785–800.

Bodnar, R.J., 1993. Revised equation and table for determining the freezing point depression of H_2O-NaCl solutions. Geochim. Cosmochim. Acta 57, 683–684.

Bodnar, R.J., Vityk, M.O., 1994. Interpretation of microthermometric data for H2O-NaCl fluid inclusions. In: De Vivo, B., Frezzotti, M.L. (Eds.), Fluid inclusions in Minerals, Methods and Applications. pp. 117–130.

Bodnar, R.J., Reynolds, T.J., Kuehn, C.A., 1985. Fluid inclusion systematics in epithermal systems. In: Berger, B.R., Bethke, P.M. (Eds.), Geology and Geochemistry of Epithermal Systems. Rev. Econ. Geol., 2, pp. 73–97.

Buchs, D.M., 2008. Late Cretaceous to Eocene geology of the South Central American forearc area (southern Costa Rica and western Panama): Initiation and evolution of an intra-oceanic convergent margin. PhD thesis Université de Lausanne, Lausanne, Switzerland (230 pp.).

Buchs, D.M., Baumgartner, P.O., Baumgartner-Mora, C., Bandini, A.N., Jackett, S.J., Diswrens, M.O., Stucki, J., 2009. Late Cretaceous to Miocene seamount accretion and melange formation in the Osa and Burica Peninsulas (southern Costa Rica); episodic growth of a convergent margin. Geol. Soc. Spec. Pub. 328, 411–456.

Buchs, D.M., Arculus, R.J., Baumgartner, P.O., Baumgartner-Mora, C., Ulianov, A.N., 2010. Late Cretaceous arc development on the SW margin of the Caribbean Plate: Insights from the Golfito, Costa Rica, and Azuero, Panama, complexes. Geochem. Geophys. Geosyst. 11, Q07S24.

Buchs, D.M., Baumgartner, P.O., Baumgartner-Mora, C., Flores, K., Bandini, A.N., 2011. Upper Cretaceous to Miocene tectonostratigraphy of the Azuero area (Panama) and the discontinuous accretion and subduction erosion along the Middle American margin. Tectonophysics 512, 31–46.

Caballero, A., 2010. Exploración de aguas subterráneas en el arco seco de Panamá (Sector de Las Tablas) mediante métodos geofísicos. PhD Thesis Universitat de Barcelona, Barcelona, Spain (271 pp.).

Clayton, R.N., Mayeda, T.K., 1963. The use of bromine pentafluoride in the extraction of oxygen from oxides and silicates for isotopic analysis. Geochim. Cosmochim. Acta 27, 43–52.

Clayton, R.N., Steiner, A., 1975. Oxygen isotope studies of the geothermal system at Wairakei, New Zealand. Geochim. Cosmochim. Acta 39, 1179–1186.

Clayton, R.N., Muffler, L.J.P., White, D.E., 1968. Oxygen isotope study of calcite and silicates of the River Ranch NO. 1 well, Salton Sea geothermal field, California. Am. J. Sci. 266, 968–979.

Corral, I., 2013. Geology and Metallogeny of the Cerro Quema Au-Cu deposit (Azuero Peninsula, Panama). PhD thesis Universitat Autònoma de Barcelona, Barcelona, Spain (211 pp.).

Corral, I., Griera, A., Gómez-Gras, D., Corbella, M., Canals, , Pineda-Falconett, M., Cardellach, E., 2011. Geology of the Cerro Quema Au-Cu deposit (Azuero Peninsula, Panama). Geol. Acta 9, 481–498.

Corral, I., Gómez-Gras, D., Griera, A., Corbella, M., Cardellach, E., 2013. Sedimentation and volcanism in the Panamanian Cretaceous intra-oceanic arc and fore-arc: New insights from the Azuero Peninsula, (SW Panama). Bull. Soc. Geol. Fr. 184, 35–45.

Corral, I., Cardellach, E., Corbella, M., Canals, , Gómez-Gras, D., Griera, A., Cosca, M.A., 2016. Cerro Quema (Azuero Peninsula, Panama): Geology, Alteration, Mineralization and Geochronology of a Volcanic Dome-Hosted High Sulfidation Au-Cu Deposit. Econ. Geol. 111, 287–310.

Del Giudice, D., Recchi, G., 1969. Geología del área del Proyecto Minero de Azuero. Informe técnico preparado para el gobierno de la República de Panamá por las Naciones Unidas. Gobierno de la República de Panamá, Panama City (Panama) (48 pp.).

Dirección General de Rercursos Minerales (DGRM), 1976. Panama Geologic Map (Mapa Geológico de la República de Panamá), scale 1:250,000. , Panama City (Panama).

Duque-Caro, H., 1990. Neogene stratigraphy, paleoceanography and paleobiogeography in Northwest South America and the evolution of the Panama Seaway. Palaeogeogr. Palaeoclimatol. 77, 203–234.

Fall, A.S., Tattitch, B., Bodnar, R.J., 2011. Combined microthermometric and Raman spectroscopic technique to determine the salinity of H_2O-CO_2-NaCl fluid inclusions based on clathrate melting. Geochim. Cosmochim. Acta 75, 951–964.

Ferencic, A., 1970. Porphyry copper mineralization in Panama. Mineral. Deposita 5, 383–389.

Field, C.W., Fifarek, R.H., 1985. Light stable-isotope systematics in the epithermal environment. In: Berger, B.R., Bethke, P.M. (Eds.), Geology and Geochemistry of Epithermal Systems. Rev. Econ. Geol., vol. 2, pp. 99–128.

Field, C.W., Gustafson, L.B., 1976. Sulfur isotopes in the porphyry copper deposit at El Salvador, Chile. Econ. Geol. 71, 1533–1548.

Field, C.W., Rye, R.O., Dymond, J.R., Whelan, J.F., Senechal, R.G., 1983. Metalliferous sediments of the East Pacific. In: Shanks III, W.C. (Ed.), Cameron Volume on Unconventional Mineral Deposits. Soc. Mining Eng. Am. Inst. Mining Metall. Petroleum Eng. pp. 133–156.

Field, C.W., Zhang, L., Dilles, J.H., Rye, R.O., Reed, M.H., 2005. Sulfur and oxygen isotopic record in sulfate and sulfide minerals of early, deep, pre-main stage porphyry Cu-Mo and late main stage base-metal mineral deposits, Butte district, Montana. Chem. Geol. 215, 61–93.

Fifarek, R.H., Rye, R., 2005. Stable isotope geochemistry of the Pierina high-sulfidation Au-Ag deposit, Peru; influence of hydrodynamics on SO_4^{2-} - H_2S sulfur isotopic exchange in magmatic-steam and steam-heated environments. Chem. Geol. 215, 253–279.

Giesemann, A., Jager, H.J., Norman, A.L., Krouse, H.R., Brand, W.A., 1994. On-line sulfur isotope determination using an elemental analyzer coupled to a mass spectrometer. Anal. Chem. 66, 2816–2819.

Giggenbach, W.F., 1992. Magma degassing and mineral deposition in hydrothermal systems along convergent plate boundaries. Econ. Geol. 87, 1927–1944.

Giggenbach, W.F., Stewart, M.K., 1982. Processes controlling the isotopic composition of steam and water discharges from steam vents and steam-heated pools in geothermal areas. Geothermics 11, 71–80.

UNCORRECTED PROOF

Gilg, H.A., Sheppard, S.M.F., 1996. Hydrogen isotope fractionation between kaolinite and water revisited. Geochim. Cosmochim. Acta 60, 529–533.
Harmon, R.S., 2005. Geological development of Panama. In: S.Harmon, R. (Ed.), The Rio Chagres, Panama. A muntidisciplinary Profile of a Tropical Watershed. 52, pp. 45–62.
Hedenquist, J.W., Garcia, J.S., 1990. Sulfur isotope systematics in the Lepanto mining district, northern Luzon, Phillippines. Min. Geol. 40, 67.
Hedenquist, J.W., Henley, R.W., 1985. The importance of CO_2 on freezing point measurements of fluid inclusions; evidence from active geothermal systems and implications for epithermal ore deposition. Econ. Geol. 80, 1379–1406.
Hedenquist, J.W., Lowenstern, J.B., 1994. The role of magmas in the formation of hydrothermal ore deposits. Nat. Geosci. 370, 519–527.
Hedenquist, J.W., Reyes, A.G., Simmons, S.F., Taguchi, S., 1992. The thermal and geochemical structure of geothermal and epithermal systems; a framework for interpreting fluid inclusion data. Eur. J. Mineral. 4, 989–1015.
Hedenquist, J.W., Matsuhisa, Y., Izawa, E., White, N.C., Giggenbach, W.F., Aoki, M., 1994. Geology, geochemistry, and origin of high sulfidation Cu-Au mineralization in the Nansatsu District, Japan. Econ. Geol. 89, 1–30.
Hoernle, K., Hauff, F., 2007. Oceanic Igneous Complexes. In: Bundschuh, J., Alvarado, G. (Eds.), Central America, geology, resources, hazards. vol. 1, pp. 523–548.
Hoernle, K., van den Bogaard, P., Werner, R., Lissinna, B., Hauff, F., Alvarado, G., Garbe-Schonberg, D., 2002. Missing history (16-71 Ma) of the Galapagos hotspot: Implications for the tectonic and biological evolution of the Americas. Geology 30, 795–798.
Holland, H.D., 1965. Some applications of thermochemical data to problems of ore deposits; Part 2, Mineral assemblages and the composition of ore forming fluids. Econ. Geol. 60, 1101–1166.
Horlacher, C.F., Lehmann, J.H., 1993. Regional Geology, Geochemistry and Exploration potential of the central Cerro Quema concession. In: Panama. Tech. Rep.. (36 pp.).
Kellogg, J.N., Vega, V., Stallings, T.C., Aiken, C.L.V., 1995. Tectonic development of Panama, Costa Rica, and the Colombian Andes; constraints from Global Positioning System geodetic studies and gravity. Geol. Soc. Am. Spec. 295, 75–90.
Kesler, S.E., Sutter, J.F., Issigonis, M.J., Jones, L.M., Walker, R.L., 1977. Evolution of porphyry copper mineralization in an oceanic island arc; Panama. Econ. Geol. 72, 1142–1153.
Kesler, S.E., Russell, N., Seaward, M., Rivera, J., McCurdy, K., Cumming, G.L., Sutter, J.F., 1981. Geology and geochemistry of sulfide mineralization underlying the Pueblo Viejo gold-silver oxide deposit, Dominican Republic. Econ. Geol. 76, 1096–1117.
Kolarsky, R.A., Mann, P., Monechi, S., Meyerhoff-Hull, D., Pessagno, E.A., 1995. Stratigraphic development of southwestern Panama as determined from integration of marine seismic data and onshore geology. Geol. Soc. Am. Spec. 295, 159–200.
Krawinkel, H., Wozazek, S., Krawinkel, J., Hellmann, W., 1999. Heavy-mineral analysis and clinopyroxene geochemistry applied to provenance analysis of lithic sandstones from the Azuero-Sona Complex (NW Panama). Sediment. Geol. 124, 149–168.
Kusakabe, M., Nakagawa, S., Hori, S., Matsuhisa, Y., Jeda, J.M., Serrano, L., 1984. Oxygen and sulfur isotopic composition of quartz, anhydrite, and sulfide minerals from the El Teniente and Rio Blanco porphyry copper deposits, Chile. Bull. Geol. Surv. Jpn 35, 583–614.
Larson, P.B., Taylor, H.P., 1987. Solfataric alteration in the San Juan Mountains, Colorado; oxygen isotope variations in a boiling hydrothermal environment. Econ. Geol. 82, 1019–1036.
Leach, T.M., 1992. Petrological Evaluation of the High Sulphidation Systems in the La Pava and Cerro Quema Prospect Areas, Panama. Tech. Rep. (55 pp.).
Lissinna, B., 2005. A profile through the Central American Landbridge in western Panama: 115 Ma Interplay between the Galápagos Hotspot and the Central American Subduction Zone. PhD thesis Christian-Albrechts Universität zu Kiel, Kiel, Germany (102 pp.).
Matsuhisa, Y., Goldsmith, J.R., Clayton, R.N., 1979. Oxygen isotopic fractionation in the system quartz–albite-anorthite–water. Geochim. Cosmochim. Acta 43, 1131–1140.
Montes, C., Bayona, G.A., Cardona, A., Buchs, D.M., Silva, C.A., Morón, S.E., Hoyos, N., Ramírez, D.A., Jaramillo, C.A., Valencia, V., 2012. Arc–continent collision and orocline formation: Closing of the Central American seaway. J. Geophys. Res. 117, B04105.
Morales-Ruano, S., Both, R.A., Golding, S.D., 2002. A fluid inclusion and stable isotope study of the Moonta copper-gold deposits, South Australia: Evidence for fluid immiscibility in a magmatic hydrothermal system. Chem. Geol. 192, 211–226.
Murray, H., Janssen, J., 1984. Oxygen isotopes - indicators of kaolin genesis?. Proc. Int. Geol. Cong. 15, 287–303.
Navarro-Ciurana, D., Corbella, M., Cardellach, E., Vindel, E., Gómez-Gras, D., Griera, A., 2016. Petrography and geochemistry of fault-controlled hydrothermal dolomites in the Riópar area (Prebetic Zone, SE Spain). Mar. Pet. Geol. 71, 310–328.
Nelson, C.E., 1995. Porphyry copper deposits of southern Central America. Arizona. Geol. Soc. Dig. 20, 553–565.
Ohmoto, H., Goldhaber, M.B., 1997. Sulfur and carbon isotopes. In: Barnes, H.L. (Ed.), Geochemistry of hydrothermal ore deposits. pp. 517–612.
Potter, R.W., Clynne, M.A., Brown, D.L., 1978. Freezing point depression of aqueous sodium chloride solutions. Econ. Geol. 73, 284–285.
Recchi, G., Miranda, R., 1977. Calizas de los Planes-Guaniquito (Tonosí). Dirección General de Recursos Minerales (DGRM), Panama City (Tech. Rep. 27 pp.).
Rye, R.O., 2005. A review of the stable-isotope geochemistry of sulfate minerals in selected igneous environments and related hydrothermal systems. Chem. Geol. 215, 5–36.
Rye, R.O., Stoffregen, R.E., Bethke, P.M., 1990. Stable isotope systematics and magmatic hydrothermal processes in the Summitville, CO, gold deposit. In: U.S. Geol. Surv. Open-File Rep. pp. 90–626.
Rye, R.O., Bethke, P.M., Wasserman, M.D., 1992. The stable isotope geochemistry of acid sulfate alteration. Econ. Geol. 87, 225–262.
Sakai, H., Matsubaya, O., 1977. Stable isotopic studies of japanese geothermal systems. Geothermics 5, 97–124.
Savin, S.M., Epstein, S., 1970. The oxygen and hydrogen isotope geochemistry of clay minerals. Geochim. Cosmochim. Acta 34, 25–42.
Savin, S.M., Lee, M., 1988. Isotopic studies of phyllosilicates. Rev. Mineral. Geochem. 19, 189–223.
Shepherd, T.J., Rankin, A.H., Alderton, D.H.M., 1985. A practical guide to fluid inclusion studies. Glasgow, United Kingdom (239 pp.).
Sheppard, S.M.F., 1986. Characterization and isotopic variations in natural waters. Rev. Mineral. 16, 165–183.
Sheppard, S.M.F., Gilg, H.A., 1996. Stable isotope geochemistry of clay minerals; The story of sloppy, sticky, lumpy and tough, Cairns-Smith (1971). Clay Miner. 31, 1–24.
Sheppard, S.M.F., Nielsen, R.L., Taylor, H.P., 1969. Oxygen and hydrogen isotope ratios of clay minerals from porphyry copper deposits. Econ. Geol. 64, 755–777.
Stoffregen, R.E., 1987. Genesis of acid-sulfate alteration and Au-Cu-Ag mineralization at Summitville, Colorado. Econ. Geol. 82, 1575–1591.
Sutcliffe, R., Kuchling, K., Burga, D., Armstrong, T., Yassa, A., Brown, F., Puritch, E., Tortelli, G., Lightwood, G., Brown, D., Gorman, M., 2014. Cerro Quema Project – Pre-feasibility study on the La Pava and Quemita oxide gold deposits. In: Prepared for Preshimco Resources Inc., by P&E Mining Consultants Inc., Golder Associates Inc., and Kappers, Cassiday and Associates. Tech. Rep. 280 pp.
Taylor, H.P., 1968. The oxygen isotope geochemistry of igneous rocks. Contrib. Mineral. Petrol. 19, 1–71.
Taylor, H.P., 1974. The Application of Oxygen and Hydrogen Isotope Studies to Problems of Hydrothermal Alteration and Ore Deposition. Econ. Geol. 69, 843–883.
Taylor, B.E., 1986. Magmatic volatiles; isotopic variation of C, H, and S. Rev. Mineral. Geochem. 16, 185–225.
Vennemann, T.W., O'Neil, J.R., 1993. A simple and inexpensive method of hydrogen isotope and water analyses of minerals and rocks based on zinc reagent. Chem. Geol. 103, 227–234.
Vennemann, T.W., Muntean, J.L., Kesler, S.E., O'Neil, J.R., Valley, J.W., Russell, N., 1993. Stable isotope evidence for magmatic fluids in the Pueblo Viejo epithermal acid sulfate Au-Ag deposit, Dominican Republic. Econ. Geol. 88, 55–71.
Wegner, W., Worner, G., Harmon, R.S., Jicha, B.R., 2011. Magmatic history and evolution of the Central American Land Bridge in Panama since Cretaceous times. Geol. Soc. Am. Bull. 123, 703–724.
Wilkinson, J.J., 2001. Fluid inclusions in hydrothermal ore deposits. Lithos 55, 229–272.

UNCORRECTED PROOF